Hierarchical Multifunctional Composites by Conformally Coating Aligned Carbon Nanotube Arrays with Conducting Polymer

Sreeram Vaddiraju,[†] Hülya Cebeci,[†,§] Karen K. Gleason,[†] and Brian L. Wardle*[,†]

Departments of Chemical Engineering and of Aeronautics and Astronautics, Massachusetts Institute of Technology; Cambridge, Massachusetts 02139, and Department of Aeronautical Engineering, Istanbul Technical University, Maslak, Istanbul 34469, Turkey

ABSTRACT A novel method for the fabrication of carbon nanotube (CNT)−conducting polymer composites is demonstrated by conformally coating extremely high aspect ratio vertically aligned-CNT (A-CNT) arrays with conducting polymer via oxidative chemical vapor deposition (oCVD). A mechanical densification technique is employed that allows the spacing of the A-CNTs to be controlled, yielding a range of inter-CNT distances between 20 and 70 nm. Using this morphology control, oCVD is shown to conformally coat 8-nm-diameter CNTs having array heights up to 1 mm (an aspect ratio of 10^5) at all inter-CNT spacings. Three phase CNT−conducting polymer nanocomposites are then fabricated by introducing an insulating epoxy via capillary-driven wetting. CNT morphology is maintained during processing, allowing quantification of direction-dependent (nonisotropic) composite properties. Electrical conductivity occurs primarily along the CNT axial direction, such that the conformal conducting polymer has little effect on the activation energy required for charge conduction. In contrast, the conducting polymer coating enhanced the conductivity in the radial direction by lowering the activation energy required for the creation of mobile charge carriers, in agreement with variable-range-hopping models. The fabrication strategy introduced here can be used to create many multifunctional materials and devices (e.g., direction-tailorable hydrophobic and highly conducting materials), including a new four-phase advanced fiber composite architecture.

KEYWORDS: chemical vapor deposition • carbon nanotubes • conducting polymer • composites • conductivity

1. INTRODUCTION

The possibility of synthesizing carbon nanotubes (CNTs) with high packing density combined with their excellent mechanical and electrical properties makes them ideal for use in a composite format for aerospace and other applications (1–11). Typically, bulk powders of CNTs are employed for the fabrication of composites by mixing them into a polymer. However, these composites are plagued by nonuniformities in composition, primarily attributable to CNT agglomeration, inhomogeneous dispersion, processes that damage the CNTs, etc. In addition, the random orientation of CNTs in these composites eliminates the possibility of realizing any direction-dependent properties. Such limitations can be avoided by synthesizing CNTs in an arrayed fashion (often referred to as vertically aligned CNT, VACNT, arrays, or forests) and then coating them conformally with a second material for obtaining composites (or elements of composites that could be processed further). Conductive-polymer coated aligned CNTs are attractive composite elements because of physical limits preventing CNT packing (i.e., the conductive polymer adds a current carrying capacity in the free space near CNTs) and because different polymers have been shown to have different conduction characteristics with the same nanomaterial reinforcement (12). Furthermore, some interesting materials for coating CNTs (e.g., inherently conducting polymers) are infusible or insoluble in any solvent and therefore must be deposited directly.

Oxidative chemical vapor deposition (oCVD) is a state-of-the-art method for the deposition of conducting polymers on nearly any substrate (13–15). In this method, both the oxidant and the monomers are supplied through the vapor phase for the deposition of conducting polymer films. Unlike chemical and electropolymerization syntheses, this method does not lead to compositional nonuniformities. oCVD is also substrate-independent, does not require the need to employ electrically conducting substrates, operates at very low temperatures (e.g., can be deposited on "tissue" paper) (13–15), and allows for the retention of chemical functionality in the coatings (e.g., −COOH-functionalized conducting polymer films can be deposited) (14). The ability to coat CNT arrays with conducting polymers is expected to allow for tuning of the conductivity and anisotropy of the composites. Further, increased conductivities are expected to be achieved even at low volume fractions in composites comprised of CNT arrays coated with conducting polymer compared to pure CNT array composites. Such anisotropic CNT−conducting polymer composites may be applied to sensors (16), field emitters (17), electrochemical capacitors (18), photovoltaic cells (19), and other devices (e.g., propulsion elements). The

* Corresponding author. E-mail: wardle@mit.edu.
Received for review July 22, 2009 and accepted September 25, 2009
† Department of Chemical Engineering, Massachusetts Institute of Technology.
‡ Department of Aeronautics and Astronautics, Massachusetts Institute of Technology.
§ Istanbul Technical University.
DOI: 10.1021/am900487z

Table 1. Conductivities and Activation Energies Required for Charge Conduction Both in the Axial and Radial Directions in A-PNCs and A-PNCs/PEDOT Composites[a]

sample[b]	intertube distance, nm	conductivity in the radial direction 30 °C, S/cm	activation energy required for charge conduction in the radial direction, eV	conductivity in the axial direction at 30 °C, S/cm	activation energy required for charge conduction in the axial direction, eV
1% CNTs/epoxy	70	0.0007	0.111	0.0004	0.085
1% CNTs/PEDOT/epoxy	50	0.002	0.080	0.003	0.040
8% CNTs/epoxy	30	0.003	0.144	0.005	0.103
8% CNTs/PEDOT/epoxy	10	0.006	0.134	0.008	0.105
20% CNTs/epoxy	20	0.005	0.101	0.008	0.121
20% CNTs/PEDOT/epoxy	<1	0.016	0.062	0.036	0.052

[a] The intertube distance always corresponds to the distance between the tubular structures both before and after coating with PEDOT (see Figure S1 in the Supporting Information). [b] CNT volume fraction given as the percent of the PNC volume occupied by CNTs.

impedance characteristics of such materials are likely even more interesting because of the anisotropy in the conducting channels and interfaces encountered.

2. EXPERIMENTAL SECTION

Multiwalled CNTs (MWNTs) were grown by thermal catalytic chemical vapor deposition (CVD) on silicon wafers using a thin catalyst layer of Fe/Al_2O_3 (1/10 nm) deposited by electron beam evaporation. CNT growth was performed in a quartz tube furnace (22 mm ID) at atmospheric pressure using ethylene as the carbon source. The nominal growth temperature was 750 °C, yielding an average growth rate (including nucleation and growth) of $\sim 2\ \mu m\ s^{-1}$ (3, 20–22). Typically, CNT arrays are grown on 1 cm^2 silicon dies, resulting in well-aligned CNTs (A-CNTs) with densities of 10^9-10^{10} CNTs cm^{-2}. As-grown CNT arrays have 1% volume fraction (1% CNTs by volume and 99% air). Deposition of poly(ethylenedioxythiophene) (PEDOT) on CNT arrays was accomplished using the well-established oCVD process (13–15). The CNT arrays were held face down in a vacuum chamber, facing the oxidizing agent. Mere heating of the oxidizing agent allowed for its sublimation into the CNT array.

EDOT was polymerized using iron chloride as the oxidant. The process involved sublimation of ~50 mg of the oxidant onto the CNTs followed by exposure to a vapor of the EDOT monomer. The duration of the entire experiment was 30 min, which includes the 5 min required for the sublimation of the oxidant onto the CNT surface. Further reaction of this incoming oxidizing agent with the EDOT monomer (supplied through the vapor phase) resulted in the formation of a PEDOT film on the CNT array substrates. All PEDOT deposition experiments were performed at a substrate temperature of 70 °C and at a pressure of 50 mTorr (13–15). Samples were gently rinsed in isopropyl alcohol following PEDOT deposition to remove any excess oxidizing agent present on the samples prior to characterization.

Following the deposition of PEDOT on the CNT arrays, these two-phase (CNT array + PEDOT) composites were lowered into a pool of epoxy and cured to obtain A-PNCs/PEDOT three-phase composites (comprised of CNTs, PEDOT, and epoxy). An aerospace-grade epoxy, RTM 6 with a viscosity of approximately 70 cP at 90 °C, was employed for this purpose (20, 23–25). The epoxy infuses into the CNT arrays through capillary-driven wetting. Following infusion of the epoxy, the composites were cured following the recommended manufacturing cure cycle (Hexcel, Duxford, U.K.). Biaxial densification is employed to vary the starting CNT–CNT spacing, and the densified CNT arrays are referred to as 8 and 20% volume fractions (see Table 1). Biaxial compression of the arrays was performed prior to both PEDOT coating or epoxy introduction in the fabrication of high volume fraction composites. The schematic that shows the definition of the intertube distance in both two- and three-phase composites is presented in Figure S1 in the Supporting Information, and the corresponding experimental intertube distances for the different volume fraction composites are given in Table 1.

Morphological and compositional characterization of the PEDOT-coated CNT arrays was performed using scanning electron microscopy (SEM), transmission electron microscopy (TEM), and energy-dispersive spectroscopy (EDS). Electrical characterization of the samples was performed using two-point probe DC measurements.

3. RESULTS AND DISCUSSION

Toward the goal of realizing anisotropic properties, multiphase composites employing conformal coatings of A-CNT arrays are presented herein. CNT arrays of ~1 mm height coated conformally with conducting polymer (PEDOT) are the key starting units to form higher-phase composites. This fabrication of uniform, conformally coated CNT arrays with inter-CNT spacings of 20–70 nm requires (i) a method for the synthesis of CNTs in an arrayed fashion over large areas and (ii) a method for obtaining conformal coating of conducting polymers on the CNT arrays without disturbing the CNT morphology. With this context, this paper demonstrates that (i) extremely high (10^5:1) aspect ratio CNT arrays can be conformally coated with conducting polymer and (ii) such composites do exhibit useful directional-dependent electrical properties. Note that intertube spacing refers to the minimum distance between adjacent CNTs, or in the case of the PEDOT coating the distance between the PEDOT coatings (see Figure S1 in the Supporting Information); e.g., 1% volume fraction CNTs have an average inter-CNT spacing of 70 nm, whereas 1% PEDOT-coated CNTs have 50 nm of intertube spacing because of the 10 nm coating on each CNT. The packing density (A-CNT volume fraction) of the CNT arrays was varied between 1 and 20% [70 to 20 nm average inter-CNT spacing (see Table 1)] via a novel mechanical densification technique (22) to explore a range of CNT array densities for conformal coating by oCVD (see Figure S2 in the Supporting Information). As-grown (1% volume fraction) CNTs are biaxially mechanically compressed after release from the growth substrate, creating uniformly increased packing of the A-CNTs (alignment has been shown to be maintained in prior work using small-angle X-ray scattering (26)). Aligned polymer nanocomposites (henceforth, referred to as A-PNCs), utilizing an insulating epoxy, are fabricated as a baseline for comparison with

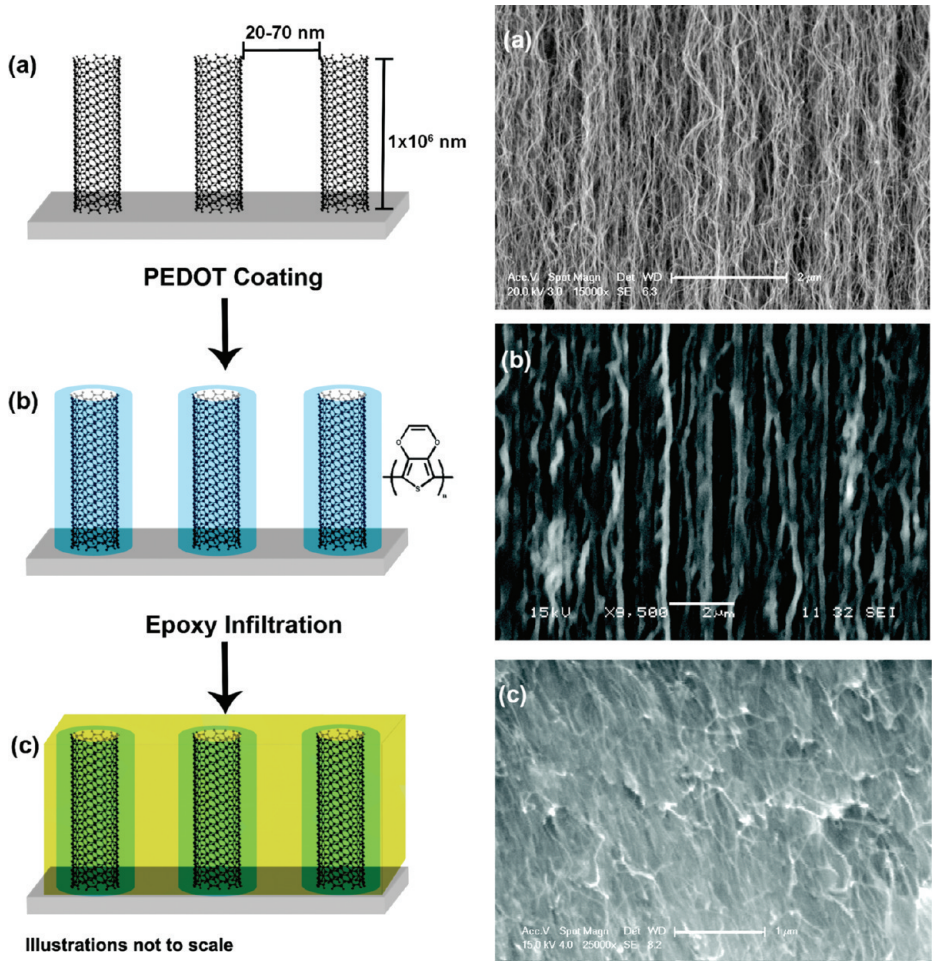

FIGURE 1. PEDOT-coated polymer nanocomposites at 1% CNT volume fraction. Illustration (left side) and micrographs (right side) of (a) A-CNTs, (b) CNTs conformally coated with PEDOT, and (c) the fracture surface of a three-phase composite after capillary-driven wetting of PEDOT-coated CNTs with an insulating polymer. The CNT array was not disturbed by either the oCVD or epoxy infiltration processes. Illustration is not to scale, especially the CNT length-to-diameter (aspect ratio) ratio, which equals 10^5.

the conducting polymer (PEDOT) coated arrays reinforced with the same epoxy (henceforth, referred to as A-PNCs/PEDOT), as illustrated in Figure 1. A-PNCs are two-phase composites (CNTs and epoxy), whereas A-PNCs/PEDOT are three-phase composites (CNTs coated with PEDOT and epoxy).

Experiments reveal that the oCVD process conformally coats the CNT arrays (of lengths >1 mm) up to the highest volume fraction attempted (20%, inter-CNT spacing of 20 nm). The process does not disturb the morphology of the CNT arrays. The electrical properties of A-PNCs/PEDOT, measured in both the axial (along the length of the CNT arrays) and radial (perpendicular to the length of the CNT arrays) directions, are found to be quite different, which demonstrates nonisotropic electrical conductivity. The conductivity in the axial direction is found to be moderately higher than that in the radial direction for both A-PNCs and A-PNCs/PEDOT (see Table 1). Further, the activation energies required for conduction in the axial direction of the composite are lower than those in the radial direction. These observations are consistent with the percolating nature of conduction in the radial direction, versus the conductive (nonpercolating) behavior expected in the axial direction, where continuous conducting CNTs span the domain of the specimen.

Polymer deposition onto CNT arrays has been reported by several groups, but conformality has not been demonstrated. These studies were mainly aimed at improving the handling of CNT arrays during composite fabrication. Notable among them are deposition of (i) parylene-C by gas pyrolysis (27), (ii) SiO_2 by CVD (28), (iii) polypyrrole (29, 30), polyaniline (31), or poly(vinyl acetate) (32) by electropolymerization, and (iv) polystyrene, poly(dimethoxysilane), or epoxies (33, 34) via capillary-driven wetting. However, these coatings have not demonstrated conformality, nor have they been shown to yield anisotropic conduction, e.g., poly(tetrafluoroethylene) on short CNT arrays using hot-filament CVD (35). Such coatings via electropolymerization lead to the shrinkage of the CNT bundles due to attractive capillary forces created during drying (as in the case of polypyrrole). It is worth noting that the diameters of the CNTs coated in the prior work are in the range of 20−60 nm and the lengths are less than 10 μm, yielding aspect ratios of less than ~100. The possibility of coating thinner (<10 nm in diameter) and longer (>1 mm in length) CNTs (aspect ratio of >100 000)

by vapor deposition of polymeric coatings has not been reported, nor have conformally coated conducting polymer nanocomposites with A-CNTs been demonstrated.

Synthesis of vertically aligned CNT arrays by thermal (21, 36–38) and plasma CVD (39), where the CNTs are oriented perpendicular to the substrate surface, have been reported. In a series of papers, Wardle et al. (20, 22, 23, 34) previously reported a method for synthesizing A-CNT polymer nanocomposites (A-PNCs) with controlled volume fraction (CNT−CNT spacing) using several unmodified polymers (22). A-PNCs were fabricated using a three-step procedure. The steps involved were as follows: (1) A-CNTs were grown using a modified CVD method on silicon substrates using an iron-on-alumina catalyst system (3, 21). The resulting A-CNTs have been characterized previously for alignment, CNT diameter, distribution, and spacing (40). The as-synthesized CNTs [referred to as 1 % volume fraction (V_f)] have densities of 10^9−10^{10} CNTs cm^{-2}. The average diameter of these CNTs is 8 nm, and the CNT−CNT spacing (center-to-center) is approximately 80 nm. (2) For high-volume-fraction PNC fabrication, the released array was then subjected to mechanical biaxial compression in two orthogonal directions. By variation of the intertube distance via compression, variable-density CNT arrays were obtained (22). (3) These (densified) arrays were then attached to a piece of adhesive carbon tape and lowered into a pool of heated and uncured polymer (22). This allowed the polymer melt to infuse into the CNT array (i.e., the polymer infused between the CNTs) via capillary-induced wetting. The rates of infusion of the polymer into the CNT array depend on characteristics of the A-CNT array (e.g., volume fraction, surface condition) and the polymer (viscosity, contact angle, etc.) (25). For the purpose of studying the directional-dependent electrical properties, the CNT−conducting polymer composite arrays were made mechanically robust by introducing an aerospace-grade insulating epoxy (RTM6, Hexcel) via capillary-driven wetting (34), followed by curing. These three-phase (CNT, PEDOT, epoxy) composites are termed A-PNCs/PEDOT as given previously.

Cross-sectional SEM images of a CNT array before and after coating with PEDOT are presented in Figure 1a,b, respectively. As observed in Figure 1a,b, the orientation and shape of the CNT bundles in the array are not disturbed by oCVD of the PEDOT coating process. Following deposition of PEDOT by oCVD, capillary-induced wetting was employed to infiltrate epoxy into the CNT/PEDOT array to create an A-PNCs/PEDOT composite. As observed in the fracture surface of Figure 1c, this capillary-induced epoxy infiltration also did not disturb the orientation of the CNTs. This is consistent with prior characterization of uncoated-CNT A-PNCs with this epoxy system, where CNT alignment and overall morphology are retained (22).

In order to confirm that each individual CNT is coated with PEDOT, these CNTs are removed from the substrate (no epoxy infiltration) and dispersed in isopropyl alcohol, and high-resolution SEM is performed. A high-magnification image of a PEDOT-coated CNT array, along with that of a single CNT coated with PEDOT, is presented in Figure 2a. These analyses showed that the diameter of PEDOT-coated CNTs is ∼30 nm (inset to Figure 2a). The diameters of the as-obtained CNTs from the array are ∼10 nm (nominal value of 8 nm). This indicates that there is a ∼10 nm thick PEDOT coating around each CNT. To further confirm the presence of PEDOT in Figure 2a, EDS analysis along the length of the PEDOT-coated CNT array is performed. A micrograph of a PEDOT-coated CNT array and a line profile of sulfur are presented in Figure 2b. The region where the sulfur line profile analysis is performed is shown in the inset to Figure 2b. The analysis shows the presence of sulfur all along the length of the CNT array. Further, the concentration of sulfur is found to be uniform all along the length of the array (Figure 2b), indicating that PEDOT deposition occurred along the length of the array and that the coating is uniform along the length. It is worth noting that the sulfur signal comes only from the PEDOT component of the composite because the as-obtained CNT arrays did not show any appreciable concentration of sulfur (see Figure S3 in the Supporting Information for an EDS sulfur profile of as-obtained CNT arrays).

In order to confirm that each individual CNT is coated with PEDOT, these CNTs are removed from the substrate (no epoxy infiltration) and dispersed in isopropyl alcohol, and TEM is performed. A comparison of TEM images of CNTs before (Figure 2c) and after PEDOT (Figure 2d) deposition clearly shows that the CNTs are coated because of their overall increased effective diameter. The 1 % volume fraction CNT arrays employed to obtain these images are synthesized and coated with PEDOT under the same conditions as those described in Figure 1a,b. The dark contrast at the edges is indicative of the presence of PEDOT around CNTs (Figure 2d). Typically, the dark contrast indicates the presence of an element with higher atomic number. Here, both oxygen and sulfur are present in PEDOT with higher atomic numbers than carbon. A high-magnification TEM image shown in Figure 2e clearly shows this contrast between the edge and center of a CNT.

Further evidence for a conformal coating of the CNT array is provided by examination of the silicon substrate after removal of the ∼1-mm-high PEDOT-coated CNTs (the procedure employed for this purpose is schematically represented in Figure S1 in the Supporting Information). If the monomer and the oxidizing agent are present all along the length of the CNT array, then PEDOT should be observed on the silicon substrate in the intertube regions. In essence, the CNT array serves as a mask. SEM analysis indicates dark regions due to PEDOT. This is confirmed by FT-IR spectroscopy (Figure 3), which confirms the presence of PEDOT coating on the silicon substrate postremoval of CNTs, as compared with a standard of PEDOT deposited on a pristine silicon wafer. Both show all of the modes typically observed in PEDOT films (see Figure 3): the vibration modes of the C−S bond at 689, 842, and 979 cm^{-1} and the ethylenedioxy ring deformation mode at 922 cm^{-1} (41). The absence of −C−H mode at 890 cm^{-1} clearly indicates that the polymerization occurred in the 2 and 5 positions. The absorption

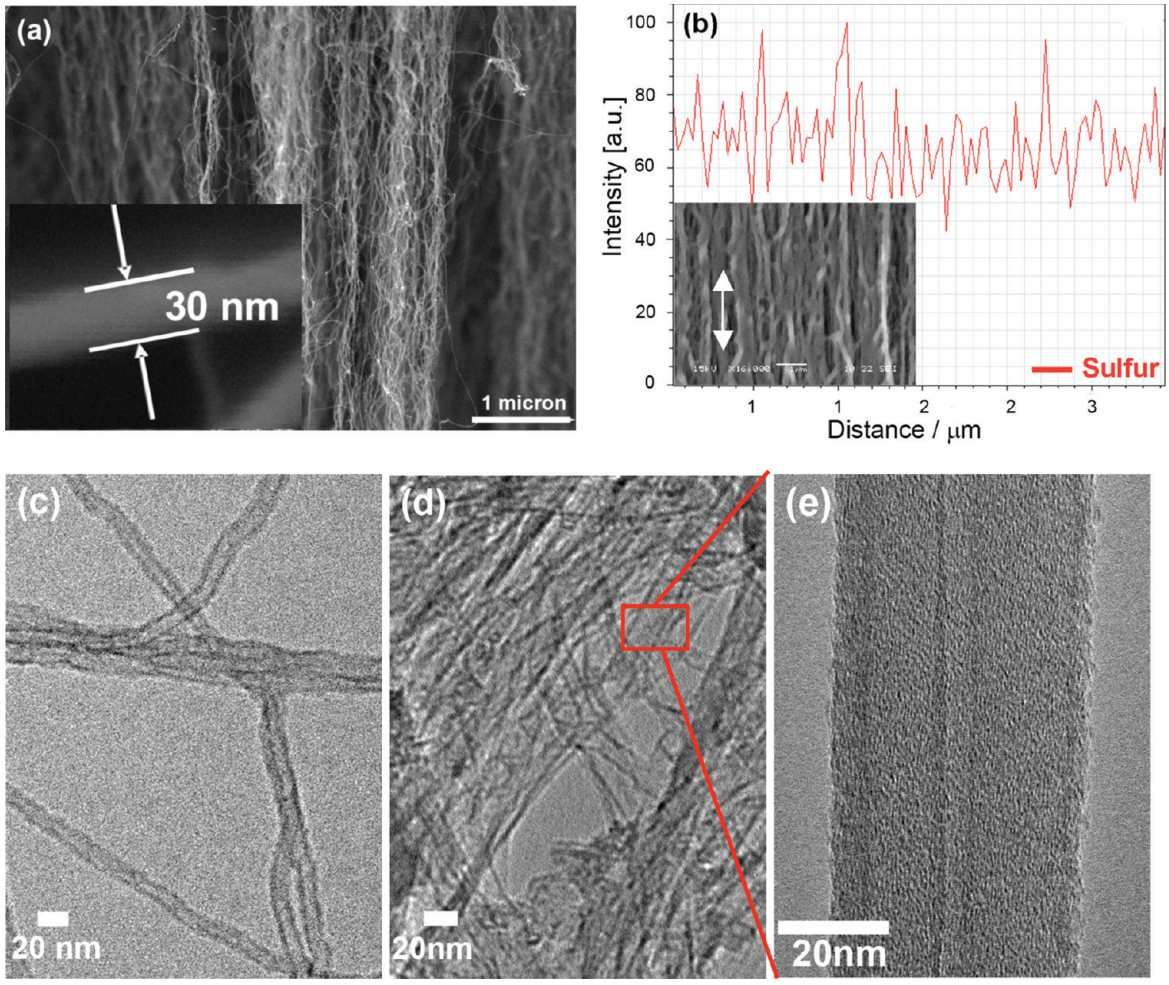

FIGURE 2. Conformal coating of CNTs. (a) Cross-sectional view of a PEDOT-coated CNT array along with a high-magnification image showing the diameter of a PEDOT-coated CNT to be ~30 nm (inset). By comparison, the diameter of as-obtained CNTs is ~10 nm. (b) Sulfur profile obtained using EDS. The sulfur concentration is observed to be uniform all along the cross section (see inset), indicating a conformal coating. TEM images of (c) as-obtained CNTs and (d) CNTs after PEDOT coating. (e) Higher magnification image of a single CNT after PEDOT coating. In addition to the increased overall diameter of the PEDOT-coated CNTs, the dark contrast at the edge in part e is indicative of the presence of PEDOT on the CNT.

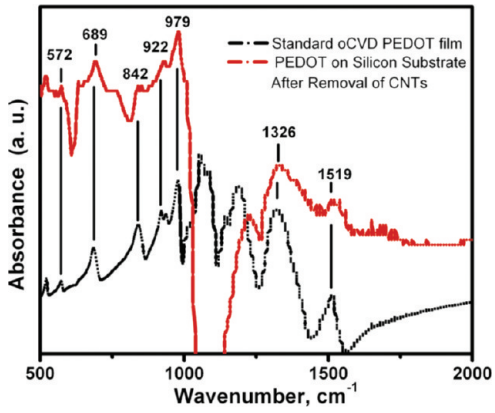

FIGURE 3. FT-IR spectrum of the silicon substrate after removal of CNTs. For comparison, a standard spectrum of oCVD deposited PEDOT film is also shown.

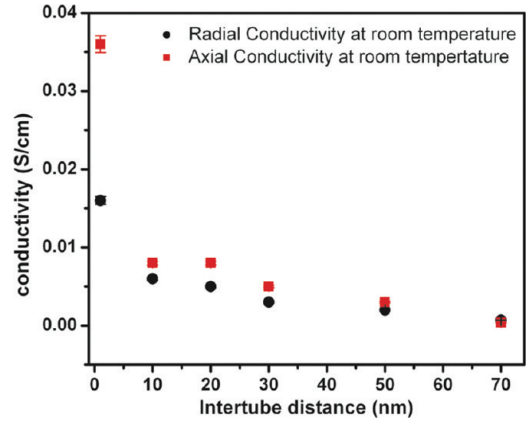

FIGURE 4. Room temperature conductivities of the A-PNCs/PEDOT composites as a function of the intertube distance in the axial and radial directions. Both the conductivity and anisotropy are found to increase with decreasing intertube distance.

at 1100 cm^{-1} (not shown in the spectra) is probably due to the formation of some silicon carbide on the substrate during the CNT growth process. Typically, the Si—O—C band is observed in the 1100 cm^{-1} region (42). These carbide peaks were not subtracted from the spectra because a silicon substrate coated with the iron catalyst was employed as the standard for obtaining the background spectra.

In order to probe the electrical behavior of the composites, the resistances of A-PNCs and A-PNCs/PEDOT compos-

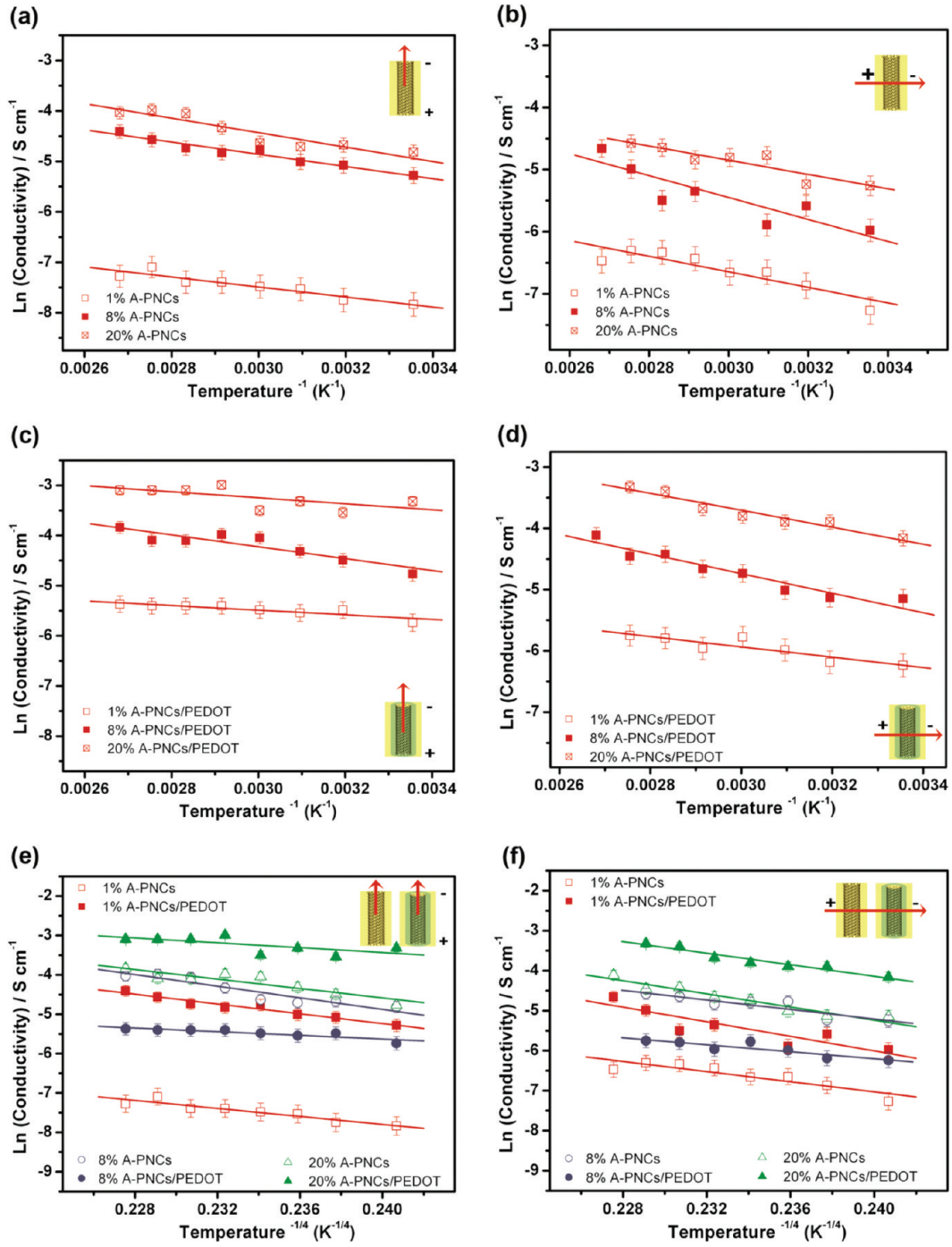

FIGURE 5. Variation in the conductivities of A-PNCs and A-PNCs/PEDOT with temperature. A-PNCs in the (a) axial and (b) radial directions and A-PNCs/PEDOT in the (c) axial and (d) radial directions. Both A-PNCs and A-PNCs/PEDOT exhibited an increase in the conductivity with temperature. Variation in the conductivities of A-PNCs and A-PNCs/PEDOT with $T^{-1/4}$ in the (e) axial and (f) radial directions. These results indicate that the conductivity is three-dimensional in both the axial and radial directions in the composites.

ites at various CNT volume fractions (inter-CNT spacings) in both the radial and axial directions are recorded as a function of the temperature. The resistance measurements were performed using two-point probe measurements, without the use of any additional metal contact pads. The resistances of the composites were then converted into bulk conductivity using the dimensions of the sample as described below.

The conductivities and intertube distances of all samples are tabulated in Table 1 and presented in Figure 4 for the three-phase A-PNCs/PEDOT composites. The conductivities of the composites in both the radial and axial directions, at a temperature of 30 °C, are found to be in the range of 0.0004−0.036 S cm^{-1}. Similar values were previously reported for polyaniline-coated CNTs and for A-PNCs with RTM6 epoxy (26, 43). The conductivity measurements of the composites suggest that introduction of PEDOT leads to an enhancement in the conductivity of the samples (Table 1). Further, a plot of the variation in the conductivity with intertube distance (Figure 4) indicates that the conductivity of the composites is always higher in the axial direction

compared to the radial direction, which is consistent with the A-PNC morphology and continuous CNT conduction paths in the axial direction, as compared to the discontinuous path(s) in the radial direction. In the radial direction, charge transfer is CNT−polymer or CNT−CNT, as opposed to simply along the CNT in the axial direction. The increase in the anisotropy of conduction in Figure 4 may be explained by the wavy nature of the A-CNTs (i.e., the CNTs are not collimated) and that this waviness decreases (improving collimation) at smaller intertube distances (26), allowing for enhanced charge conduction along the CNT axis.

In order to further understand the anisotropic behavior in conductivity, the variations in the conductivity of A-PNCs and A-PNCs/PEDOT samples with temperature are recorded and presented in Figure 5a−d. Parts a and b of Figure 5 are Arrhenius plots of the variation of conductivities with temperatures in the A-PNCs in the axial and radial directions, respectively. A-PNCs are observed to exhibit an increase in the conductivity with an increase in the temperature. Similar plots for A-PNCs/PEDOT (Figure 5c,d) also showed the same behavior. The activation energy required for charge conduction is deduced from these plots and presented in Table 1. The activation energy for charge conduction in the radial direction is found to be higher than those corresponding to the axial direction. This result is expected because the conductivity in the axial direction occurs along the length of the CNTs and hence a continuous path for charge conduction exists. However, no continuous path for conduction exists through the CNTs in the radial direction, consistent with the observation that conductivities in the radial direction are lower, and activation energies higher, in the radial direction. In all cases (see Table 1 and Figure 5), PEDOT increases the conductivity of the composite and decreases the activation energy relative to composites (A-PNCs) without PEDOT.

In order to further understand the conductivity behavior in the composites, variation in the conductivity with the temperature was modeled using the variable-range-hopping (VRH) model. Typically, percolation theory (19) is employed to explain the conductivity in CNT composites. However, this theory assumes that a conductive path exists or is created due to electron hopping and/or tunneling in the composite between the CNTs. However, in both the axial and radial directions, CNT volume fraction is at least 10× higher than that needed for percolation even at 1 % volume fraction, and therefore percolation theory is not relevant (it is certainly not relevant in the axial direction where continuous CNTs span the sample domain). VRH models were employed to understand the conductivity behavior in the composites. According to the VRH model, conductivity occurs by hopping of charge carriers and the conductivity (σ) follows the following relationship with temperature (44, 45).

$$\sigma = \sigma_0 e^{-(T_0/T)^{1/n+1}} \quad (1)$$

Here, T_0 is the characteristic temperature and n is the dimensionality of the conduction. The best fit of the conductivity with temperature is found for $n = 3$ for both the axial (Figure 5e) and radial (Figure 5f) directions in both the A-PNCs and A-PNCs/PEDOT samples. This indicates that the conductivity occurs by hopping of charge carriers in three dimensions in both the radial and axial directions. This may be explained easily in the radial direction and in the axial direction by the fact that the CNT arrays have regions where the CNTs are not oriented perfectly perpendicular to the substrate; i.e., the CNTs are wavy instead of collimated. These wavy CNTs lead to both contact and entanglements, and hence the conductivity is three-dimensional in both the axial and radial directions. However, the conductivity is dominated by the CNTs in the axial direction, and hence the activation energy required for charge conduction is lower in the axial direction. This could be avoided by employing CNTs with slightly lower densities (lower than the 1 % volume fraction or 10^{10} CNTs cm^{-2} arrays currently employed) for composite fabrication.

Last, a skeleton is fabricated that can form the basis for a four-phase advanced composite: A-CNTs are grown radially on the surface of micrometer-diameter (aerospace standard) fibers and then coated conformally via oCVD. The SEM images in Figure S4 in the Supporting Information show that the A-CNT morphology can be preserved upon coating with PEDOT via oCVD. Further work to infiltrate this skeleton with epoxy and assess the multifunctional performance attributes is underway.

4. CONCLUSIONS

In summary, a method for the fabrication of composites by conformally coating A-CNT arrays by conducting polymer through an oCVD process is presented. The oCVD process preserves the morphology and structure of the CNT arrays. In addition to enhancing the conductivity, this process can be used to tailor and design directional-dependent properties of the composites. Conductivity measurements of A-PNCs and A-PNC/PEDOT displayed anisotropic behavior in the composites, with higher conductivities in the axial direction. The measurements also indicated that both the conductivity and anisotropy could be tuned through variations in the intertube distance. Further, the activation energies required for charge conduction are found to be lower in the axial direction compared to the radial direction. Although the conductivity is found to be three-dimensional in the composites, the conductivity is dominated by the CNTs in the axial direction and not in the radial direction. The conformal coatings demonstrated here can be used to form interesting multifunctional structures such as thermal-interface materials and electrical connections for sensing applications, in addition to providing a route to creating four-phase multifunctional composites (23, 46).

Acknowledgment. This study was supported by Airbus S.A.S., Boeing, Embraer, Lockheed Martin, Saab AB, Spirit AeroSystems, Textron Inc., Composite Systems Technology, and TohoTenax Inc. through MIT's Nano-Engineered Composite Aerospace STructures (NECST) Consortium. H.C. acknowledges support from the Scientific and Technical Research Council of Turkey (TUBITAK) for a NATO-A2 Sci-

ence Fellowship. The authors gratefully acknowledge Patrick Boisvert (MIT) for SEM imaging and Fevzi Cakmak Cebeci (MIT) for TEM imaging.

Supporting Information Available: Schematic representation of procedure to characterize the conformality of PEDOT coating onto CNT arrays. Illustrations of mechanical densification, EDS profile of sulphur on an as grown CNT array, SEM image of A-CNTs grown onto woven alumina fibers with and without PEDOT coating to form a skeleton for four phase. This material is available free of charge via the Internet at http://pubs.acs.org.

REFERENCES AND NOTES

(1) Schadler, L. S.; Kumar, S. K.; Benicewicz, B. C.; Lewis, S. L.; Harton, S. E. *MRS Bull.* **2007**, *32*, 335–340.
(2) Thostenson, E. T.; Ren, Z. F.; Chou, T. W. *Compos. Sci. Technol.* **2001**, *61*, 1899–1912.
(3) Garcia, E. J.; Hart, A. J.; Wardle, B. L. *AIAA J.* **2008**, *46*, 1405–1412.
(4) Coleman, J. N.; Khan, U.; Blau, W. J.; Gun'ko, Y. K. *Carbon* **2006**, *44*, 1624–1652.
(5) Dresselhaus, M. G.; Dresselhaus, G.; Eklund P. C. *Science of Fullerenes and Carbon Nanotubes*; Academic Press: New York, 1996.
(6) Futaba, D. N.; Hata, K.; Yamada, T.; Hiraoka, T.; Hayamizu, Y.; Kakudate, Y.; Tanaike, O.; Hatori, H.; Yumura, M.; Iijima, S. *Nat. Mater.* **2006**, *5*, 987–994.
(7) Koziol, K.; Vilatela, J.; Moisala, A.; Motta, M.; Cunniff, P.; Sennett, M.; Windle, A. *Science* **2007**, *318*, 1892–1895.
(8) Treacy, M. M. J.; Ebbesen, T. W.; Gibson, J. M. *Nature* **1996**, *381*, 678–680.
(9) Winey, K. I.; Vaia, R. A. *MRS Bull.* **2007**, *32*, 314–319.
(10) Yu, M. F.; Lourie, O.; Dyer, M. J.; Moloni, K.; Kelly, T. F.; Ruoff, R. S. *Science* **2000**, *287*, 637–640.
(11) Zhang, M.; Fang, S. L.; Zakhidov, A. A.; Lee, S. B.; Aliev, A. E.; Williams, C. D.; Atkinson, K. R.; Baughman, R. H. *Science* **2005**, *309*, 1215–1219.
(12) Bauhofer, W.; Kovacs, J. Z. *Compos. Sci. Technol.* **2009**, *69*, 1486–1498.
(13) Im, S. G.; Yoo, P. J.; Hammond, P. T.; Gleason, K. K. *Adv. Mater.* **2007**, *19*, 2863+.
(14) Lock, J. P.; Im, S. G.; Gleason, K. K. *Macromolecules* **2006**, *39*, 5326–5329.
(15) Vaddiraju, S.; Senecal, K.; Gleason, K. K. *Adv. Funct. Mater.* **2008**, *18*, 1929–1938.
(16) Santhosh, P.; Manesh, K. M.; Gopalan, A.; Lee, K. P. *Anal. Chim. Acta* **2006**, *575*, 32–38.
(17) Jin, Y. W.; Jung, J. E.; Park, Y. J.; Choi, J. H.; Jung, D. S.; Lee, H. W.; Park, S. H.; Lee, N. S.; Kim, J. M.; Ko, T. Y.; Lee, S. J.; Hwang, S. Y.; You, J. H.; Yoo, J. B.; Park, C. Y. *J. Appl. Phys.* **2002**, *92*, 1065–1068.
(18) Sivakkumar, S. R.; Ko, J. M.; Kim, D. Y.; Kim, B. C.; Wallace, G. G. *Electrochim. Acta* **2007**, *52*, 7377–7385.
(19) Kymakis, E.; Amaratunga, G. A. J. *Appl. Phys. Lett.* **2002**, *80*, 112–114.
(20) Garcia, E. J.; Hart, A. J.; Wardle, B. L.; Slocum, A. H. *Adv. Mater.* **2007**, *19*, 2151.
(21) Hart, A. J.; Slocum, A. H. *J. Phys. Chem. B* **2006**, *110*, 8250–8257.
(22) Wardle, B. L.; Saito, D. S.; Garcia, E. J.; Hart, A. J.; de Villoria, R. G.; Verploegen, E. A. *Adv. Mater.* **2008**, *20*, 2707–2714.
(23) Garcia, E. J.; Wardle, B. L.; Hart, A. J.; Yamamoto, N. *Compos. Sci. Technol.* **2008**, *68*, 2034–2041.
(24) Wardle, B. L.; Hart, A. J.; Garcia, E. J.; Saito, D. S.; Cebeci, H., MIT, 2008.
(25) Cebeci, H.; Guzman de Villoria, R.; Wardle, B. L.; Saito, D. S.; Yamamoto, N.; Ishiguro, K.; Garcia, E. J.; Hart, A. J.; Wicks, S. *SAMPE Fall Technical Conference*, Memphis, TN, Sept 2008.
(26) Cebeci, H.; de Villoria, R. G.; Hart, A. J.; Wardle, B. L. *Compos. Sci. Technol.* **2009**, online Sept. 2009.
(27) Miserendino, S.; Yoo, J.; Cassell, A.; Tai, Y. C. *Nanotechnology* **2006**, *17*, S23–S28.
(28) Li, J.; Stevens, R.; Delzeit, L.; Ng, H. T.; Cassell, A.; Han, J.; Meyyappan, M. *Appl. Phys. Lett.* **2002**, *81*, 910–912.
(29) Chen, J. H.; Huang, Z. P.; Wang, D. Z.; Yang, S. X.; Li, W. Z.; Wen, J. G.; Ren, Z. F. *Synth. Met.* **2001**, *125*, 289–294.
(30) Nguyen-Vu, T. D. B.; Chen, H.; Cassell, A. M.; Andrews, R. J.; Meyyappan, M.; Li, J. *IEEE Trans. Bio-Med. Eng.* **2007**, *54*, 1121–1128.
(31) Gao, M.; Huang, S. M.; Dai, L. M.; Wallace, G.; Gao, R. P.; Wang, Z. L. *Angew. Chem., Int. Ed.* **2000**, *39*, 3664–3667.
(32) Wei, C.; Dai, L. M.; Roy, A.; Tolle, T. B. *J. Am. Chem. Soc.* **2006**, *128*, 1412–1413.
(33) Sansom, E. B.; Rinderknecht, D.; Gharib, M. *Nanotechnology* **2008**, *19*, -.
(34) Garcia, E. J.; Hart, A. J.; Wardle, B. L.; Slocum, A. H. *Nanotechnology* **2007**, *18*, -.
(35) Lau, K. K. S.; Bico, J.; Teo, K. B. K.; Chhowalla, M.; Amaratunga, G. A. J.; Milne, W. I.; McKinley, G. H.; Gleason, K. K. *Nano Lett.* **2003**, *3*, 1701–1705.
(36) Hata, K.; Futaba, D. N.; Mizuno, K.; Namai, T.; Yumura, M.; Iijima, S. *Science* **2004**, *306*, 1362–1364.
(37) Reina, A.; Hofmann, M.; Zhu, D.; Kong, J. *J. Phys. Chem. C* **2007**, *111*, 7292–7297.
(38) Jung, Y. J.; Wei, B. Q.; Vajtai, R.; Ajayan, P. M. *Nano Lett.* **2003**, *3*, 561–564.
(39) Melechko, A. V.; Merkulov, V. I.; McKnight, T. E.; Guillorn, M. A.; Klein, K. L.; Lowndes, D. H.; Simpson, M. L. *J. Appl. Phys.* **2005**, *97*, -.
(40) Hart, A. J.; Slocum, A. H. *Nano Lett.* **2006**, *6*, 1254–1260.
(41) Lin-Vien, D.; Colthup, N. B.; Fateley, W. B.; Grasselli, J. G. *Infrared and Raman Characteristic Frequencies of Organic Molecules*; Academic Press: New York, 1991.
(42) Zhang, S.; Pereira, L.; Hu, Z.; Ranieiro, L.; Fortonato, E.; Ferreira, I.; Martins, R. *J. Non-Cryst. Solids* **2006**, *352*, 1410–1415.
(43) Long, Y. Z.; Chen, Z. J.; Zhang, X. T.; Zhang, J.; Liu, Z. F. *Appl. Phys. Lett.* **2004**, *85*, 1796–1798.
(44) Maddison, D. S.; Unsworth, J.; Roberts, R. B. *Synth. Met.* **1988**, *26*, 99–108.
(45) Mott, N. F. *Adv. Phys.* **1967**, *16*.
(46) Wicks, S. S.; de Villoria, R. G.; Wardle, B. L. *Compos. Sci. Technol.* **2009**, online Oct. 2009.

AM900487Z